GEOPHYSICS, VOL. 62, NO. 5 (SEPTEMBER-OCTOBER 1997); P. 1419–1431, 15 FIGS.

Inversion of geophysical data over a copper gold porphyry deposit: A case history for Mt. Milligan

Douglas W. Oldenburg*, Yaoguo Li*, and Robert G. Ellis*

ABSTRACT

In this paper, we invert magnetic, DC resistivity, induced polarization (IP), and airborne electromagnetic (EM) data from the Mt. Milligan copper-gold porphyry deposit and jointly interpret the inversion results with available geological and mineralization data. The inversions are carried out over an area that encloses an intrusive stock, known as the MBX Stock, and the resulting mineralization zone surrounding it. The earth model is discretized into a large number of cells having constant physical properties, and distributions of magnetic susceptibility, conductivity, and chargeability are obtained by minimizing a model objective function subject to adequately fitting the corresponding data. A 3-D magnetic susceptibility model is obtained directly by inverting surface total field anomaly data. 3-D conductivity and chargeability models are formed by compositing 2-D sections recovered by inverting DC/IP pole-dipole data. The airborne EM data are inverted with a 1-D algorithm and composited into a 3-D conductivity model. The physical property models are compared with a rock model constructed from geologic information from 600 drill holes and with a 3-D model of gold concentration. The physical property models have features that correlate with various geologic boundaries and rock units. More notably, the recovered chargeability and susceptibility seem to reflect the distribution of mineralization: chargeability highs coincide with the greatest gold concentration, while the susceptibility displays an anticorrelation with it.

Overall, our inversion results are consistent with the geology and mineralization models for the Cu-Au porphyry deposit, while the anticorrelation between gold concentration and susceptibility provides an important constraint that helps define the distribution and geochemical control of the orebody.

THE MT. MILLIGAN DEPOSIT

Mt. Milligan is a Cu-Au porphyry deposit situated in north central British Columbia. The deposit lies within the Early Mesozoic Quesnel Terrane that hosts a number of Cu-Au porphyry deposits and it occurs within porphyritic monzonite stocks and adjacent volcanic rocks of the Takla group. Extensive knowledge about the geology and mineralization has been achieved through a major drilling program. The initial deposit model consists of a vertical monzonitic stock intruding into a volcanic host. Dykes extend out from the stock and cut through the porous trachytic units in the host. The original structure and mineralization essentially displayed a symmetry about the vertical axis but subsequent geologic activity has caused the system to rotate 45° eastward and the whole system is further complicated by faulting and erosion.

Emplacement of a monzonite intrusive stock is accompanied by intensive hydrothermal alteration primarily in the region near the boundaries of the stock and in and around the porous trachytic units. A general model for porphyry systems, taken from McMillan (1991) and reproduced in Figure 1, shows that both potassic and propylitic alteration can be expected. Potassic alteration, which produces chalcopyrite, bornite and magnetite, occurs in a region surrounding the initial stock and its intensity decreases away from the boundary. The initial stock contains accessory magnetite and alteration products and these would be expected both in the host and in the intrusive. Propylitic alteration, which produces pyrite and minor amounts of magnetite, exists outwards from the potassic alteration zone. It is expected that the pyrite content increases markedly as one proceeds from a potassic to a propylitic alteration zone. For the MBX deposit at Mt. Milligan the simple conceptual pattern of

Manuscript received by the Editor December 11, 1995; revised manuscript received December 23, 1996.
*UBC—Geophysical Inversion Facility, Dept. of Earth and Ocean Sciences, University of British Columbia, 129–2219 Main Mall, Vancouver, British Columbia, Canada V6T 1Z4. E-mail addresses: doug@geop.ubc.ca and li@geop.ubc.ca.

potassic alteration occurring close to the stock and in the trachytic units, and propylitic alteration occurring in a broad halo surrounding the potassic alteration is complicated by the reality that there were a number of alteration events with different locations, intensities, and time scales. It is also likely that there was overprinting of propylitic alteration in regions that had already undergone potassic alteration and vice versa.

The individual rock units and alteration products have physical properties that can be detected with geophysical surveys. Magnetite content will alter the magnetic susceptibility; pyrite, chalcopyrite, and bornite affect chargeability; and significant mineralization and fluid filled fractures will alter the electrical conductivity. Geophysical surveys have the potential to provide quantitative information about the distribution of these physical properties, and magnetic, DC resistivity, IP, and airborne EM data have been collected at Mt. Milligan. In this study we concentrate on a 1.2 km $\times$ 1.0 km area over the top of the MBX East deposit. We begin with a general description of our inversion methodology and then proceed with the inversion of magnetic, DC resistivity, IP, airborne EM data. The recovered physical property models are then compared with the rock and Au mineralization models found by direct sampling. Comparisons suggest an unexpected correlation between abundances of magnetite, pyrite, and gold. This issue is discussed and we also use this hypothesis to carry out cooperative inversions of the magnetic and IP data.

INVERSION METHODOLOGY

Individual geophysical data sets at Mt. Milligan are inverted by using standard approaches in inverse theory. The earth is divided into rectangular cells having constant physical properties. The number of cells generally greatly exceeds the number of data, and in general, there are many distributions of the physical property which, when forward modeled, produce predicted responses that are in adequate agreement with the observations. To confront this nonuniquess the inverse problem is formulated so as to minimize an objective function of the model subject to adequately fitting the data. To some degree, the output of the inversion algorithm depends upon the choice of objective function and an important aspect of our inversions involves decisions regarding which objective function should be minimized for each problem. Generally we choose to find minimum structure models since these are more easily interpreted, but the generalized objective function used here allows flexibility to generate a variety of models and also to incorporate additional information into the inversion process.

The magnetic data have been inverted using a 3-D algorithm, the DC resistivity and IP data have been inverted using a 2-D algorithm, and the airborne EM data have been inverted using a 1-D algorithm. The method adopted for solving individual inverse problems depends upon the size of the matrix to be inverted and the amount of computational effort required to form individual sensitivities. For 1-D problems, the matrix equations can be solved with direct methods, while for 2-D problems and for the 3-D magnetic problem we have used a generalized subspace method. Nevertheless all inversions can be cast into the following methodology.

Let the data be denoted generically by the symbol d and the model by m. To carry out forward modeling to generate theoretical responses, and also to attack the inverse problem,

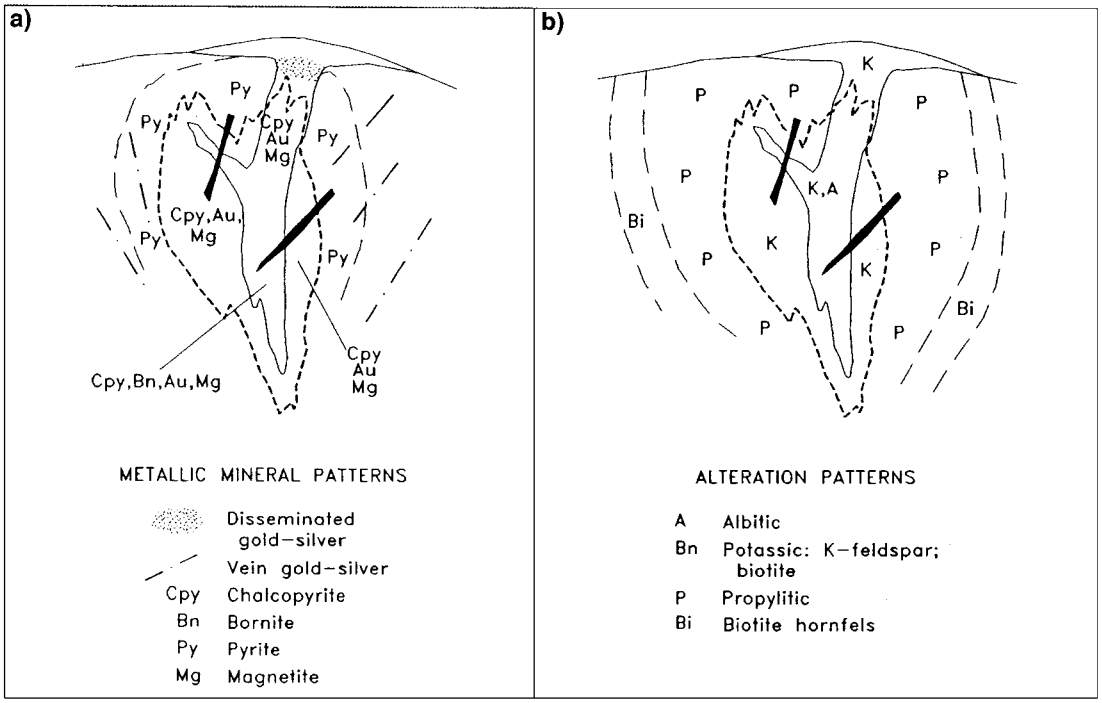

FIG. 1. Mineralization system associated with a typical Cu-Au Porphyry system extracted from McMillan (1991). Diagram (a) indicates the metallic mineral distribution. The solid line in the middle represents the initial stock. The areas of potassic and propylitic alteration are shown in (b).

we divide our model domain into M rectangular cells and assume that the physical property is constant within each cell. Our inverse problem is solved by finding the vector $\mathbf{m} = \{m_1, m_2, \ldots, m_M\}$ which adequately reproduces the observations $\mathbf{d}_0 = (d_{01}, d_{02}, \ldots, d_{0N})$.

The inverse problem is posed as a standard optimization problem:

$$\begin{aligned} &\text{minimize} && \psi_m(\mathbf{m}, \mathbf{m}_0) = \|\mathbf{W}_m(\mathbf{m} - \mathbf{m}_0)\|^2 \\ &\text{subject to} && \psi_d(\mathbf{d}, \mathbf{d}_0) = \|\mathbf{W}_d(\mathbf{d} - \mathbf{d}_0)\|^2 = \psi_d^*. \end{aligned} \tag{1}$$

In equation (1) $\mathbf{m}_0$ is a base model and $\mathbf{W}_m$ is a general weighting matrix that is designed so that a model with specific characteristics is produced. The minimization of the model objective function ψ_m yields a model that is close to $\mathbf{m}_0$ with the metric defined by $\mathbf{W}_m$ and so the characteristics of the recovered model are controlled directly by these two quantities. The choice of ψ_m is crucial to the solution of the inverse problem but we defer the details until later. $\mathbf{W}_d$ is a datum weighting matrix. We shall assume that the noise contaminating the jth observation is an uncorrelated Gaussian random variable having zero mean and standard deviation ϵ_j. As such, an appropriate form for the $N \times N$ matrix is $\mathbf{W}_d = diag\{1/\epsilon_1, \ldots, 1/\epsilon_N\}$. With this choice, ψ_d is the random variable distributed as chi-squared with N degrees of freedom. Its expected value is approximately equal to N and accordingly, ψ_d^*, the target misfit for the inversion, should be about this value. The appropriate objective function to be minimized is

$$\psi(\mathbf{m}) = \psi_m(\mathbf{m}, \mathbf{m}_0) + \mu\big(\psi_d(\mathbf{d}, \mathbf{d}_0) - \psi_d^*\big), \tag{2}$$

where μ is a Lagrange multiplier.

Because of nonuniqueness the character of the final model is heavily influenced by the model objective function. Our choice for ψ_m is guided by the fact that we often wish to find a model that has minimum structure in the vertical and horizontal directions and at the same time is close to a base model m_0. This model, because it is "simple" in some respect, may be representative of the major earth structure. Other earth models however, might be closer to reality and it is necessary that the objective function have the capability to produce a variety of models and be flexible enough to incorporate additional information that the interpreter has about the model. An objective function that can accomplish these goals is

$$\psi_m(m, m_0) = \alpha_s \int_{vol} w_s(m - m_0)^2\, dv + \int_{vol} \left\{ \alpha_x w_x \left(\frac{\partial (m - m_0)}{\partial x} \right)^2 + \alpha_y w_y \left(\frac{\partial (m - m_0)}{\partial y} \right)^2 + \alpha_z w_z \left(\frac{\partial (m - m_0)}{\partial z} \right)^2 \right\} dv. \tag{3}$$

In equation (3) the functions w_s, w_x, w_y, w_z are specified by the user, the constant α_s controls the importance of closeness of the constructed model to the base model m_0, and α_x, α_y, α_z control the roughness of the model in the horizontal and vertical directions. The discrete form of equation (3) is

$$\begin{aligned} \psi_m &= (\mathbf{m} - \mathbf{m}_0)^T \big\{ \alpha_s \mathbf{W}_s^T \mathbf{W}_s + \alpha_x \mathbf{W}_x^T \mathbf{W}_x \\ &\quad + \alpha_y \mathbf{W}_y^T \mathbf{W}_y + \alpha_z \mathbf{W}_z^T \mathbf{W}_z \big\} (\mathbf{m} - \mathbf{m}_0) \\ &\equiv (\mathbf{m} - \mathbf{m}_0)^T \mathbf{W}_m^T \mathbf{W}_m (\mathbf{m} - \mathbf{m}_0) \end{aligned} \tag{4}$$

and this defines the matrix $\mathbf{W}_m$ in equation (1). The base model can be omitted from any of the terms in equation (3) if desired.

INVERSION OF MAGNETIC DATA

In a ground based magnetic survey at Mt. Milligan, total field data were collected at 12.5 m intervals along east-west lines spaced 50 m apart. A regional field, derived from data taken over a larger area, was removed from the observations and the reduced data were then down-sampled to a 25 m interval to form the final set of 1029 observations. The data were upward continued to a height of 20 m in accordance with our practice of inverting magnetic data at a height that is about equal to a cell dimension. These data are shown in Figure 2. Each datum is assigned a standard error of 5% plus 10 nT. To invert these data, we first discretize the 1.2 km by 1.0 km by 450 m model domain into cells having constant, but unknown, susceptibilities. Cell widths are 25 m in the horizontal directions and thickness varies from 12.5 to 25 m. Surrounding this core region, the model is extended laterally outward by two large cells so that the resultant model consists of 43 428 cells. Topography that varies by about 100 m over the area was included in the modeling.

The magnetic field at Mt. Milligan is $H_0 = 58\,193$ nT, $I = 75^\circ$ and $D = 25.7^\circ$. We assume that there is no remanent magnetization contributing to the observations and that demagnetization effects are negligible. Consequently, the relationship between the total field anomaly data and the susceptibility is given by

$$\mathbf{G}\kappa = \mathbf{d}, \tag{5}$$

where the matrix $\mathbf{G}$ has elements G_{ij} which quantify the contribution to the ith datum due to a unit susceptibility in the jth cell. The model objective function is that given in equation (3) with the exception that an additional depth weighting function, based upon the natural decay of the elements of $\mathbf{G}$, is applied to each component. This is a crucial aspect of the objective function since it causes the recovered susceptibilities to be distributed with depth whereas without it, the susceptibilities tend to be biased toward the surface. To invoke the inverse methodology we set $m = \kappa$, $m_0 = 0$, and $(\alpha_s, \alpha_x, \alpha_y, \alpha_z) = (.0005, 1., 1., 1,)$. The resultant system of equations is solved using a subspace technique with a requirement that the susceptibility remain positive. Further details and discussion regarding the magnetic inversion algorithm are given in Li and Oldenburg (1996).

Figure 3 displays one plan view and three vertical cross-sections of the recovered susceptibility. From the plan section, two concentrated susceptibility highs are observed in the central region. Surrounding them are three linear anomalies trending northeast. In the cross-sections, the major anomalies are seen at moderate depth but considerable variation in the depth to the top is evident. There are also smaller anomalies extending to the surface. In general, the models show more

detailed structure near the surface and become smoother at depth.

INVERSION OF DC RESISTIVITY DATA

The pole-dipole DC resistivity and IP surveys over Mt. Milligan were carried out along east-west lines spaced 100 m apart. The dipole length was 50 m and data for $n = 1$ to 4 were collected. This yields a total of 86 data for each line.

The governing equation for the dc resistivity potentials is

$$\nabla \cdot (\sigma \nabla \phi) = -I\delta(r - r_s), \tag{6}$$

where σ is the electrical conductivity and r_s denotes the location of the current electrode. To invert the DC data, we adopt a 2-D assumption and invert data from each line separately. Equation (6) is a nonlinear relationship between the observed potentials and the conductivity and hence an iterative technique is used. We use the subspace technique outlined in Oldenburg et al. (1993). The model objective function is that given in equation (3) with neglect of the y-variable and volumetric integrals replaced by areal integrals over x and z. Since conductivity varies over orders of magnitude and is also positive we choose $m = \ell n\sigma$ as the variable in the inversion. The reference model is a uniform half-space of 1.67 mS/m and $(\alpha_s, \alpha_x, \alpha_z) = (.0002, 1.0, 1.0)$. The model is discretized into 1600 cells with cells in the central region of the section having a width of 25 m and a thickness of 10 m.

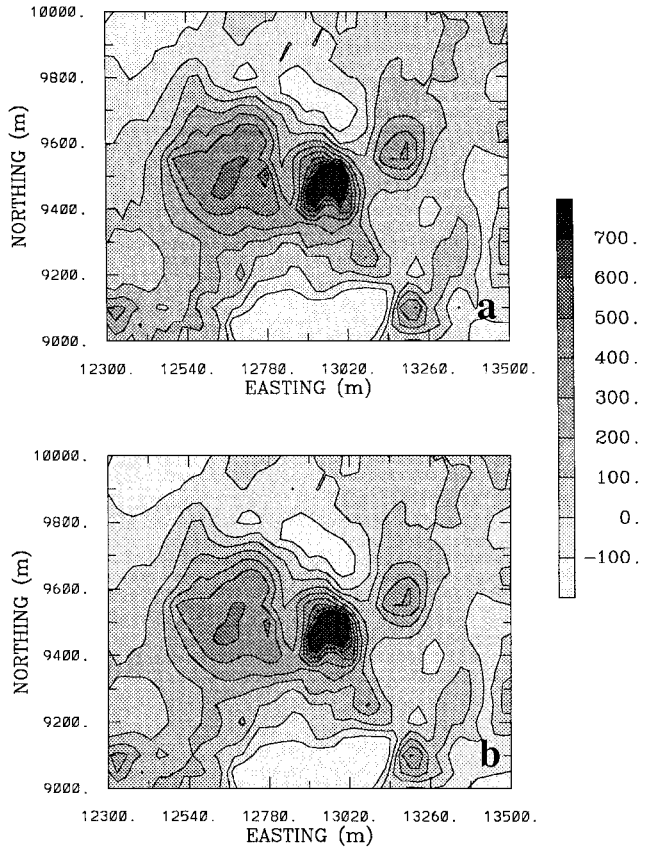

FIG. 2. The magnetic data to be inverted are shown in the top panel. The predicted responses from the inverted model are shown below. The grey scale is in nT.

There are 86 observations for each survey line and each datum is assumed to have a standard error of 5%. An example of the data, shown as an apparent conductivity pseudosection, is given in Figure 4. Depth information is difficult to infer from this plot, and lineations are caused principally by the pole-dipole nature of data collection. The inverted conductivity model, shown in that figure, has a central resistive zone with high conductivities on both sides. Conductive features are limited to depths of about 100 m. Features below this do not significantly affect the data and the conductivity approaches that of the base model. This limited depth of investigation of about 100 m is in accordance with the fact that the maximum distance between the current electrode and potential electrode is 250 m. The predicted data are shown in Figure 4 and agree well with the observations. Eleven east-west lines spaced at 100 m intervals were inverted and the resulting models were combined to form a composite 3-D model. One plan view and three cross-sections are shown in Figure 5. The individual inversions did not include topography effects but for display purposes the resultant conductivity sections have been vertically

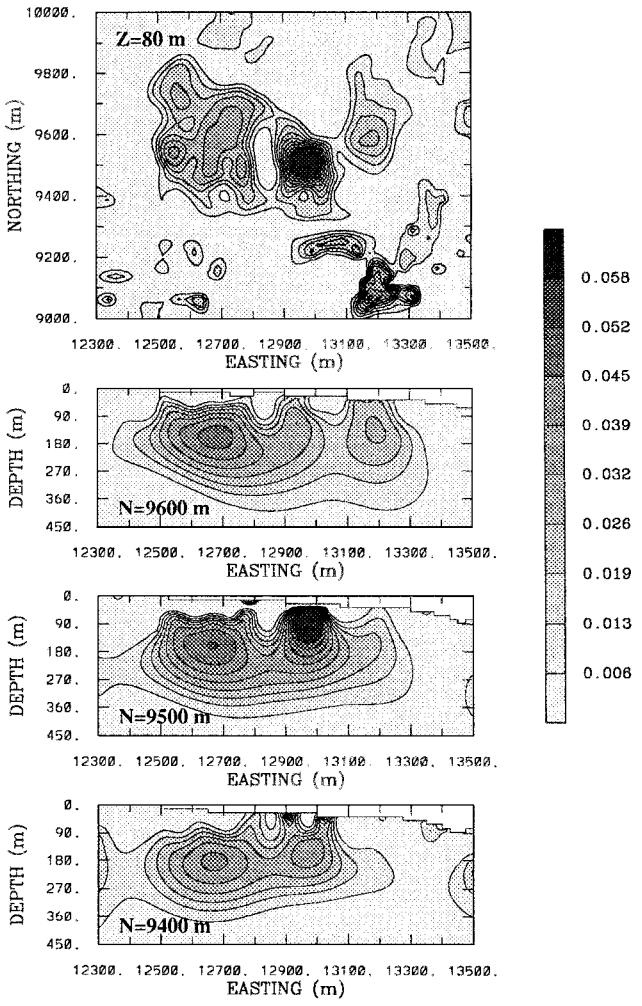

FIG. 3. A plan view of the inverted magnetic susceptibility at a depth of $z = 80$ m is shown at the top. Three east-west cross-sections at $x = 9400$, 9500, and 9600 m are given below. The grey scale is magnetic susceptibility in SI units.

adjusted by the local topography. This is a valid methodology since topography is minor and limited to gentle slopes.

INVERSION OF IP DATA

IP data were collected simultaneously with the DC resistivity data. The secondary potentials have been converted to apparent chargeabilities and an example pseudosection for the 9600N line is shown in Figure 6. Each datum is assigned a constant standard deviation that is about 5% of the average of all IP data. Inversion of IP data is a two-step process. In the first step, DC resistivity data are inverted to generate a background conductivity. By making the assumption that the chargeabilities, represented by the symbol η, are small then the relationship between the apparent and intrinsic chargeabilities is given by

$$\eta_a = \mathbf{J}\eta. \tag{7}$$

In equation (7) J_{ij} is ijth element of the sensitivity matrix for the DC resistivity problem. That is, $J_{ij} = -\partial \ell n \phi^i[\sigma]/\partial \ell n \sigma_j$ where σ is the conductivity model obtained from the dc inversion. The second step of the IP inversion solves a linear inverse problem using equation (7) as the constraints.

The cell discretization and model objective function for the IP inversion are identical to those used in the DC resistivity inversion. However, the background model is set to zero and the model parameter chosen for the inversion is $m = \eta$. Positivity on chargeability is invoked using the subspace technique and details regarding the inversion can be found in Oldenburg and Li (1994).

The recovered chargeability model at line 9600N is shown in Figure 6. There is a strong chargeable zone at depth toward the east and another chargeable zone near the surface to the west. The predicted data shown in that figure agree well with the observations. Depth limitations for the IP structure are the same as those for DC resistivity and hence chargeable features are seen only to about 100 m depth. Inversions for the eleven lines were carried out and composited to form a 3-D model. One plan view and three cross-sections are shown in Figure 7.

INVERSION OF AIRBORNE EM DATA

A DIGHEM airborne EM survey was flown in north-south lines 100 m apart. In-phase and phase data at frequencies 900, 7200, 56 000 Hz were taken about every 10 meters along the flight line. The six data at each source location were inverted using a 1-D inversion algorithm to produce a conductivity depth distribution. In performing this operation the earth was divided into 14 layers and the model objective function was that given in equation (3) but now relegated to 1-D so $\alpha_x = \alpha_y = 0$.

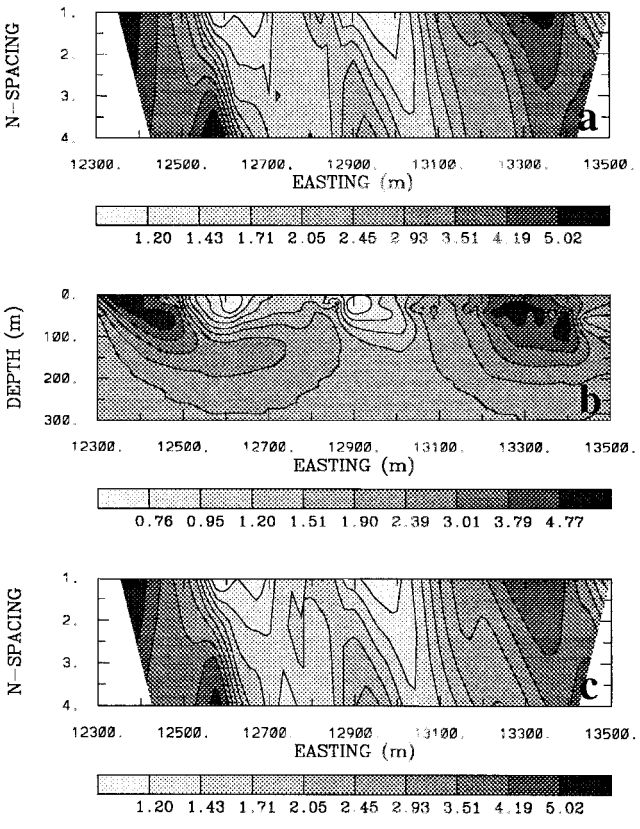

FIG. 4. The apparent conductivity data for $n = 1, 4$ for a pole-dipole survey at 9600N are shown at the top. The recovered conductivity obtained from the 2-D inversion is shown in the middle panel and the predicted data are given at the bottom. The grey scale denotes conductivities in mS/m.

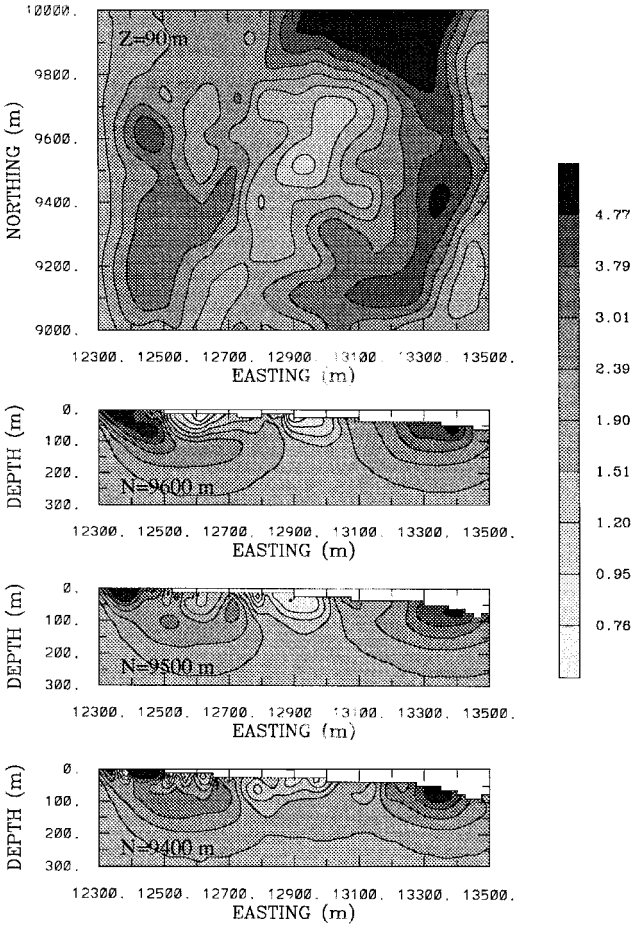

FIG. 5. A plan view of the electrical conductivity at $z = 90$ m obtained from inverting dc resistivity data is shown at the top. Three east-west cross-sections at $x = 9400$, 9500, and 9600 m are given below. The grey scale denotes conductivities in mS/m.

The model parameter for inversion was $m = \log\sigma$, the reference model corresponded to a halfspace of 3.16 mS/m and $(\alpha_s, \alpha_z) = (0.4, 0.6)$. The in-phase and quadrature data at 900, 7200, 56 000 Hz data were assigned respective errors of 20, 25, 70, 50, 65, and 50 DIGHEM units. The high magnetite content in the rocks caused in-phase values to decrease and, in certain locations, to become negative. In an attempt to minimize the contaminating effect of magnetic susceptibility on the conductivity inversion, we thresholded the data so that the minimum in-phase datum value was 5.3 for 900 Hz and 64 for 7200 Hz. These thresholds correspond to in-phase values obtained for a half-space of 1.67 mS/m and hence should be characteristic of the lowest values expected.

Rather than attempting to fit each data set to the same degree, we have carried out all inversions by minimizing the same objective function $\phi = \phi_m + \mu\phi_d$. This is a useful procedure when inverting many data sets in which the errors are not known as they are in this case since the 1-D assumption is assuredly violated. The reader is referred to Ellis and Shekhtman (1994) for more detailed information about the inversion. The results of the 1-D inversions carried along a line 12625 E are shown in Figure 8. The observed and predicted data, shown at the top are in relatively good agreement. The conductivity model is at the bottom. Carrying out the 1-D inversion for the eleven north-south lines and compositing the results yields a 3-D model. One plan view and three cross-sections of the conductivity model are shown in Figure 9. Comparing these conductivities with those in the top 100 m in Figure 5 shows reasonable agreement in the general features.

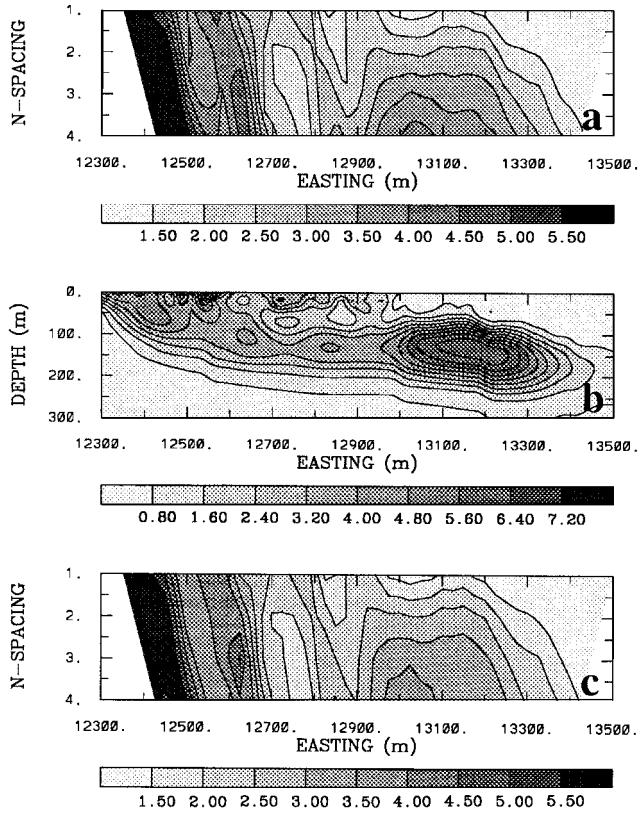

FIG. 6. The apparent chargeability data for $n = 1, 4$ for a pole-dipole survey at 9600N are shown at the top. The recovered chargeability obtained from the 2-D inversion is shown in the middle panel and the predicted data are given at the bottom. The grey scale denotes chargeabilities in percent.

ROCK MODEL, GEOLOGIC CROSS-SECTIONS AND GOLD MODEL

Validation of our inversions is ideally made if in-situ measurements of physical properties are available. Unfortunately, none exist at Mt. Milligan, and therefore we look for correlations with available geologic and mineralization data. Geologic logs from 600 drill holes in the analysis region were used to construct a 3-D rock model that contained overburden, fault location, and five of the most common rock types including monzonite, trachytes, and latites. A cross-section at 9600N is shown in Figure 10. The major elements are: (1) the monzonite stock that is truncated on the left by the Harris Fault, (2) the arcuate feature, called the Rainbow Dyke, extending from the stock to the surface on the right, and (3) trachyte dykes between the Rainbow dyke and the central monzonite unit. In addition to our rock model, we obtained a geologic cross-section at 9600N

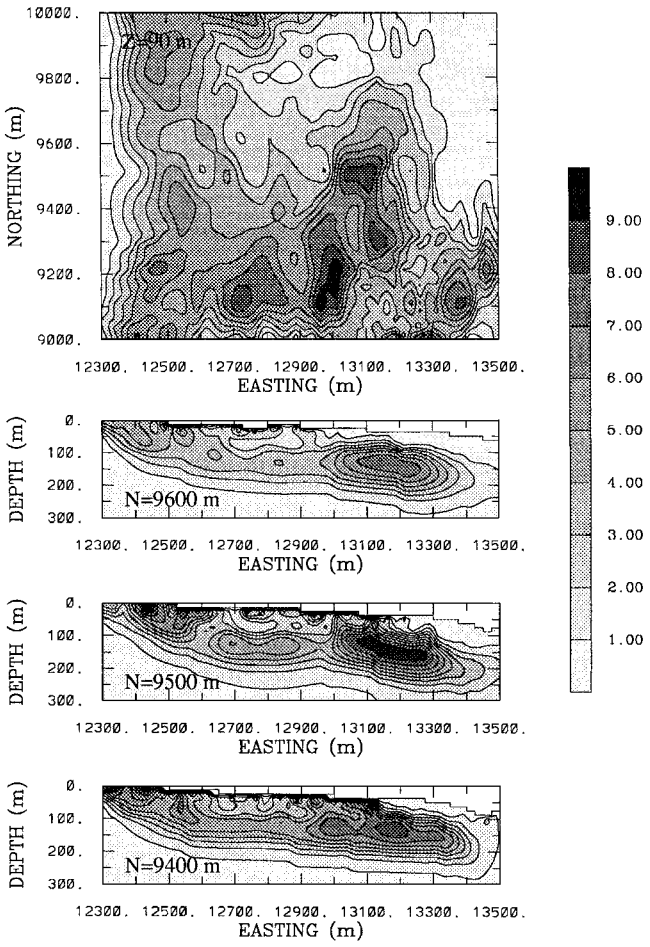

FIG. 7. A plan view of chargeability at $z = 90$ m obtained from inverting IP data is shown at the top. Three east-west cross-sections at $x = 9400$, 9500, and 9600 m are given below. The grey scale denotes chargeabilities in percent.

from DeLong et al. (1995), and this is reproduced in Figure 10. In DeLong's cross-section, the trachyte dykes are more clearly visible, and they have about a 45° plunge that corresponds approximately to the rotation that the porphyry deposit has undergone subsequent to the initial emplacement of the stock and mineralization. The reasonable agreement between major features in our rock cross-section and the DeLong model provides confidence that either of these geologic descriptions can be used in our interpretation. Subsequent diagrams will use both as overlays.

Also available for comparison is a 3-D Au model for the MBX deposit that was composited from assayed values of drill core. The Au grade is given in categories 1 through 4, with 4 being the highest. Figure 11 displays the Au contours in plan view and in cross-sections.

JOINT INTERPRETATION OF GEOPHYSICAL, GEOLOGICAL, AND MINERALIZATION DATA

Our information base consists of: (1) a rock model constructed from drill logs and a geologic cross-section at 9600N; (2) conductivity models from DC resistivity and airborne EM inversions; (3) chargeability from IP inversion; (4) susceptibility from magnetic inversion; and (5) a 3-D gold distribution. It is expected that our inversion results may be correlated with the rock type or they may be correlated with alteration products. We examine both of these possibilities.

Figure 12 displays respectively the overlay of essential geological features on the recovered conductivities, chargeability, and susceptibility. Major features such as the Harris Fault, MBX Stock, Rainbow Dyke are identified by the labels. On the

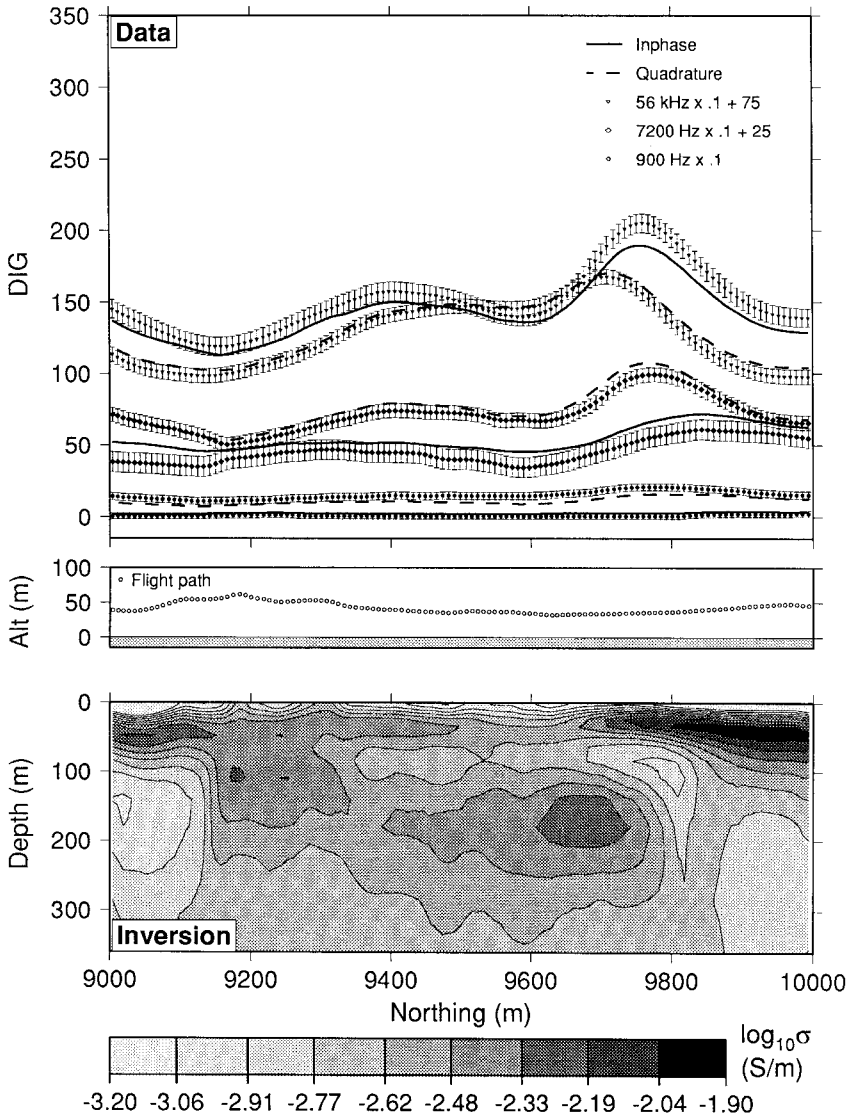

FIG. 8. Conductivities obtained by carrying out 1-D inversion along the line 12625E. Observed data are plotted with assigned error bars and in-phase and quadrature predicted data are plotted in solid and dashed lines, respectively. (◇, △, ○) refer respectively to 56 000, 7200, and 900 Hz. The conductivity is given at the bottom. The height of the receiver above the ground, as recorded by an altimeter, is given in the middle.

conductivity section that is recovered from the DC resistivity data and shown in Figure 12a, high conductivities are observed at, and to the left of, the Harris Fault. East of the fault one observes low conductivities associated with the monzonite stock. Higher conductivities are again observed in the volcanics to the east of where the Rainbow Dyke reaches the surface. The conductivity obtained from the 1-D inversion of AEM data, and shown in Figure 12d, shows the same general features. High chargeabilities shown in Figure 12b are observed westward of the Harris Fault and in an area centered around the Rainbow Dyke. The location of high chargeabilities on the left and right hand sides of the picture is consistent with the hypothesis that the initial stock and mineralization had a vertical axis of symmetry and that the entire unit has been rotated clockwise and eroded at the surface. The recovered susceptibility section in Figure 12c shows high values associated with the monzonite stock. This is expected because of the initial magnetite content of the stock. There is also a susceptibility low in the area enclosed by the Rainbow Dyke.

Comparison of the inversion results and mineralization is shown by superimposing the gold concentration onto the recovered conductivity, chargeability, susceptibility, and rock model. The superposition of gold concentration onto the conductivity section is shown in Figure 13a. The red and pink contours (categories 3 and 4) coincides with low to intermediate conductivities. Prior to alteration, the stock was resistive compared to its volcanic host. The final conductivity in this region appears to be substantially greater than that of the initial stock but it is still relatively small. There is a substantial increase in gold concentration beneath the conductive feature on the east. Superposition of gold concentration onto the chargeability section is shown in Figure 13b. There is a general correlation between chargeability and gold concentration. It is noted that the major concentration of gold lies slightly to the left of the major concentration of chargeability. This offset may be typical for Cu-Au porphyry deposits. That is, higher Au values tend to be found toward the stock, where concentrations of chalcopyrite are large, compared to the high regions of chargeability away from the stock that are related more to pyrite content. Superposition of gold onto the magnetic susceptibility in Figure 13c indicates that the region of high gold values corresponds to a low susceptibility, or equivalently, to low magnetite concentrations. The superposition of gold concentration onto the rock model is shown in Figure 13d. The high value gold contours are centered on the boundary between the stock and the host. This is an area where intense hydrothermal activity has occurred.

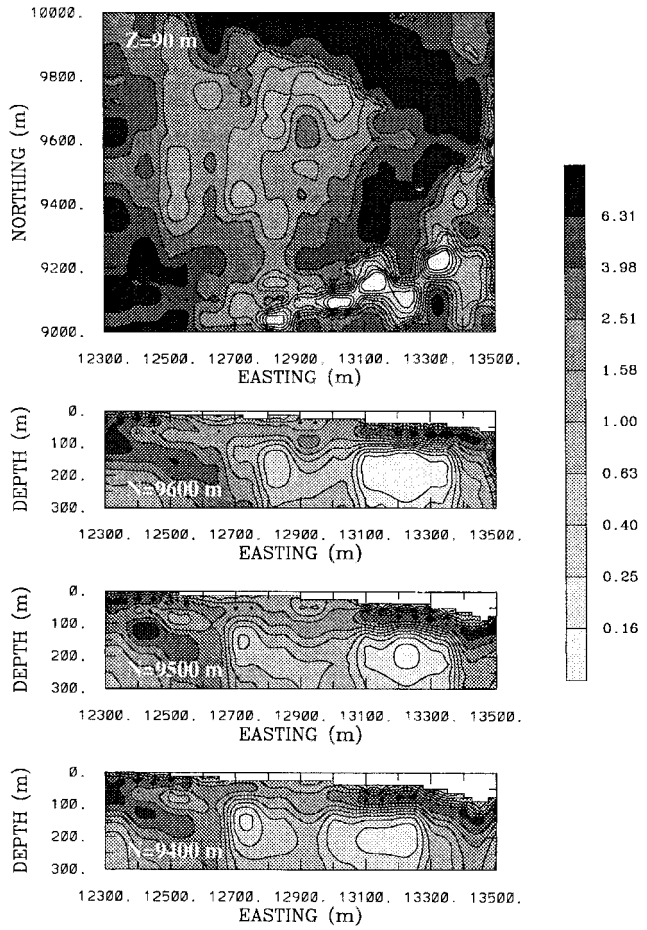

FIG. 9. A plan view of the electrical conductivity at $z = 90$ m obtained from inverting airborne EM data is shown at the top. Three east-west cross-sections at $x = 9400$, 9500, and 9600 are given below. The grey scale denotes conductivities in mS/m.

GEOCHEMICAL CONSTRAINT FROM GEOPHYSICAL INVERSIONS

The high Au concentration in the Rainbow dyke region is associated with relatively low susceptibility and high chargeability. The existence of low susceptibility and high gold concentration in this region is supported by visual estimates of magnetite concentrations from four drill holes in the area. (DeLong, pers. comm., 1994). The low susceptibility found from our inversion caused Stanley (pers. comm., 1996) to modify and refine a thermodynamic model for mineralization and hydrothermal alteration at Mt. Milligan. Briefly, previous thermodynamic models (DeLong, 1991) suggested that two stages of alteration (potassic and propylitic) occurred at the MBX East deposit where our geophysical studies have been carried. The first stage, which is valid for the entire MBX deposit area, involved a reaction between a high temperature (>350°) aqueous fluid and the host rock to produce potassic alteration (K-spar, biotite, epidote, magnetite). Au and Cu were transported in these fluids as chloride complexes, and deposition of Au and Cu took place via the following chemical reactions:

$$\mathrm{CuCl_2^- + Fe^{+2} + 2H_2S \rightarrow CuFeS_2 + 2Cl^- + 4H^+ + e^-}$$
$$\mathrm{AuCl_2^- + e^- \rightarrow Au^0 + 2Cl^-}. \quad (8)$$

Au and chalcopyrite are hypothesized to have been precipitated because of the cooling of the hydrothermal fluid. Because the saturation ratio of these Cu and Au chloride complexes is relatively temperature insensitive, the resulting Cu/Au ratio of mineralized rock is predicted to be relatively constant. This is illustrated by the bubbleplot in Figure 14 of Cu and Au values from the MBX West Zone that is adjacent to the MBX East Zone. These data plot with relatively high correlation with a mode that is approximated by a line through the origin that corresponds to a Cu/Au ratio of 15 000. That value is consistent with the Cu/Au chloride complex saturation ratio in the

hypothesized hydrothermal fluid for temperatures above 350°. In summary, for this first stage potassic alteration, we would expect that Cu/Au ratios would be relatively constant near 15 000, and areas with high Cu and Au grades would be associated with high susceptibility because of an abundance of magnetite and with moderate chargeability because of the presence of chalcopyrite.

At the MBX East Zone, where our analysis was carried out, it was observed that the Cu/Au ratios are significantly lower than those at the MBX West Zone (see Figure 14) despite the fact that the mode for this assay population is also 15 000 (Stanley, 1993). To account for this, it was postulated that a second stage, lower temperature, event occurred. At lower temperatures, Au forms a strong bisulphide (HS^-) complex, but Cu does not and Au-only precipitation was thought to occur via the reaction:

$$Au(HS)_2^- + Fe^{+2} \rightarrow Au^0 + FeS_2 + 2H + e^-. \qquad (9)$$

This would decrease the Cu/Au ratio and increase the chargeability because of the added pyrite but it would not alter the susceptibility. The low susceptibilities seen in the inversion model, and which coincided with the region of highest gold concentration, thus presented an enigma. Stanley's (pers. communication, 1996) resolution was to hypothesis that the Au precipitation probably occurred alone during propylitic alteration (chlorite, pyrite, epidote) by the following reaction in which magnetite is converted to pyrite:

$$Au(HS)_2^- + Fe_3O_4 \rightarrow Au^0 + FeS_2 + [Fe_2O_3] + H_2O + e^-. \qquad (10)$$

The ferric iron produced by this reaction is taken up in epidote, which has been omitted in this reaction because of the balancing complexity introduced by the additional elements in epidote. Textural evidence supporting this reaction (pyrite and epidote, with gold, replacing magnetite) has been observed in the adjacent 66 Zone at Mt. Milligan (DeLong, pers. comm., 1994). This reaction would decrease the Cu/Au ratio through the addition of Au, increase the chargeability through the addition of pyrite, and lower the susceptibility through the destruction of magnetite and formation of epidote. Both of these geophysical predictions are in accordance with the inversion results.

The geophysical inversion results are therefore shown to be consistent with the two stage process of a new thermodynamic model for mineralization and hydrothermal alteration at Mt. Milligan. This consistency is of mutual benefit as predictions from one study are corroborated by those of the other. From our perspective it provides additional confidence that the geophysical inversions are producing meaningful results.

COOPERATIVE INVERSION

An initial objective with the Mt. Milligan data was to carry out joint and/or cooperative inversion of the various data sets to arrive at a final geological model that is compatible with all of the data. By "cooperative inversion" we mean using information from one data set to affect the inversion of another data set. Computationally, the output of a first inversion is incorporated as a weighting in the objective function in equation (3) and then the second inversion is performed. As an example

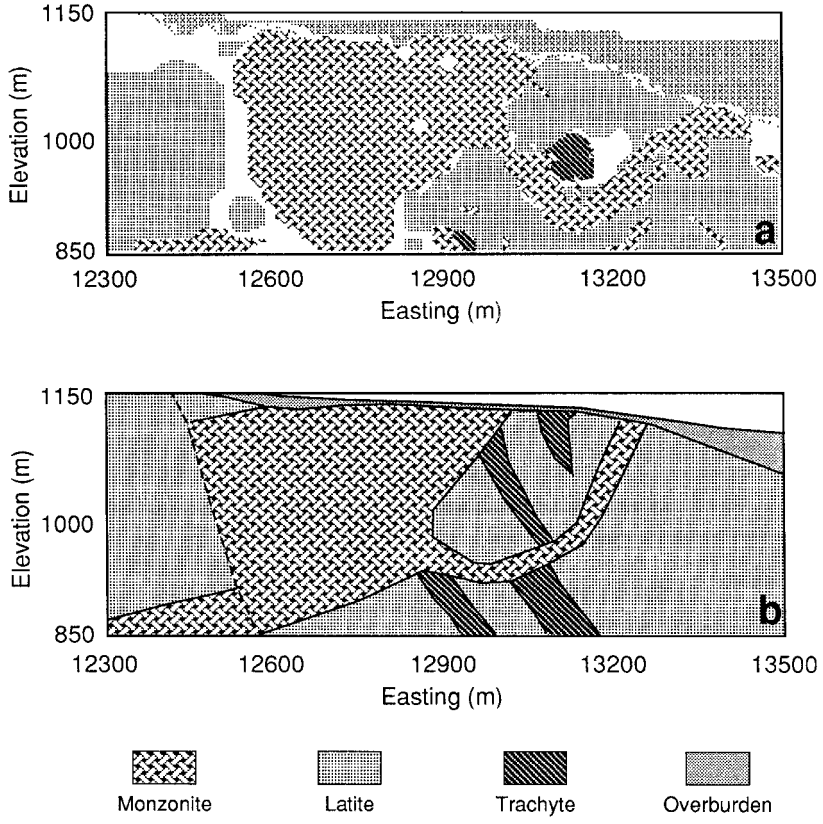

FIG. 10. Cross-section at 9600N of the 3-D rock model obtained from data from 600 drill holes is shown at the top. The geologic section from DeLong is shown below.

we carry out a cooperative inversion that was stimulated by the results in Figure 13 and the geochemical analysis in the previous section. In the region of the Rainbow dyke there is relatively low susceptibility and high chargeability. Furthermore the stock tends to have high susceptibility and low chargeability. This leads to a hypothesis that there is a general anticorrelation between chargeability and susceptibility. We adopt this hypothesis. Cooperative inversions then can be carried out by using the distribution of chargeability as a weighting when inverting the magnetic data or using the distribution of susceptibility as a weighting when inverting the IP data. We show the latter here. The inverted magnetic susceptibility is scaled to the range (0, 1) and used as a weighting function w_s in equation (3) in the inversion of IP data. The cross-section of the weighting function at 9600N is shown in Figure 15. The weighting function is 1.0 in the region where the susceptibility is small, and it increases to 10.0 at the center of the susceptibility high. This weighting function forces the IP inversion to place chargeability away from regions of high magnetic susceptibility if the resulting model still adequately fits the data. We have carried out the weighted inversion using an approximate 3-D IP inversion algorithm, and the cross-section at 9600N is shown in Figure 15. For comparison the same cross-section obtained from the generic inversion without weighting is also shown. In the weighted inversion the chargeability is moved toward the surface and the single anomaly in the generic inversion is split into two parts.

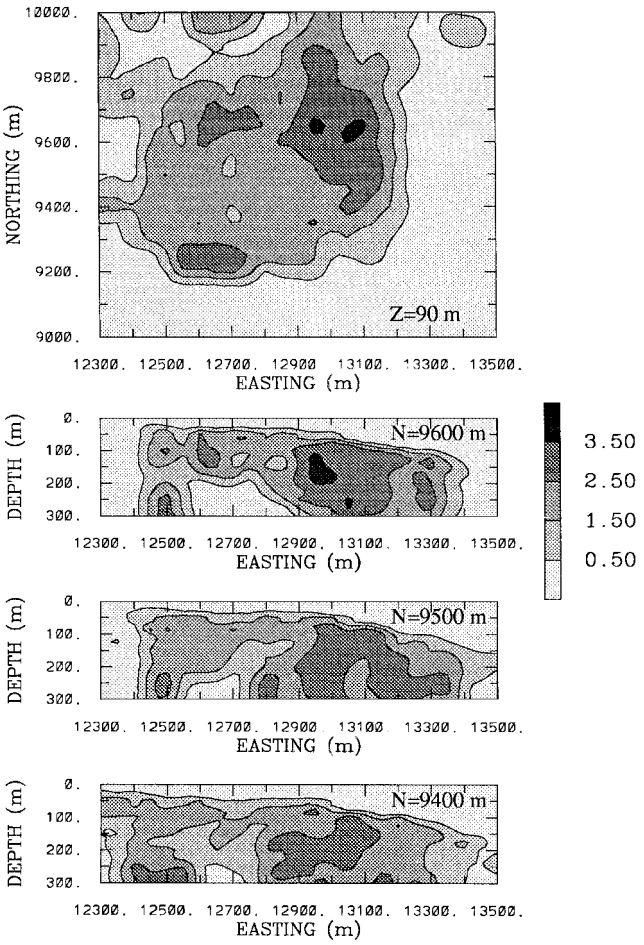

FIG. 11. A plan view of gold concentration at $z = 90$ m obtained from drill holes is shown at the top. Three east-west cross-sections at $x = 9400$, 9500, and 9600 m are given below. The grey scale denotes gold concentration that has been binned into categories 1 through 4, with 4 indicating the highest value.

CONCLUSION

The Mt. Milligan deposit area is complex both from a geologic perspective and because of its history of alteration episodes. Physical properties are affected by rock type and by alteration state, and thus making inferences about either rock type or mineralization directly from the geophysical data is not easily done. In this paper, we have inverted four geophysical data sets from Mt. Milligan to recover 3-D distributions of physical properties. The distribution of electrical conductivity is useful in differentiating between the monzonitic stock and the host material and also in delineating fault regions. The combination of conductivity and susceptibility provides good estimates for location of the intrusive stock. Chargeability is governed primarily by amounts of chalcopyrite and pyrite. The most intensive gold deposition should be associated with potassic alteration close to the stock and in dykes extending from the stock. Both pyrite and chalcopyrite are associated with this potassic alteration. However, pyrite concentration might be expected to increase away from the stock as one enters regions of propylitic alteration. The greatest chargeability may therefore be expected to lie somewhat outboard of the primary mineralization. We note that even drilling the chargeability high along the line 9600N would have found the major gold region in the Rainbow Dyke area. Additionally, the geophysical inversion results in the MBX East Zone support a recent thermodynamic model for Cu-Au porphyry deposits in which a second stage low temperature event deposited Au in a reaction that consumed magnetite. Combining all of the above information leads to a model in which the location of largest Au concentration should be associated with relatively low magnetic susceptibility and that the highest Au concentration should lie inboard from the chargeability high. A drill hole, spotted on the basis of this joint interpretation of the geophysical and geological data, would have penetrated the area of the highest gold concentration.

ACKNOWLEDGMENTS

This work was supported by an NSERC IOR grant and an industry consortium "Joint and Cooperative Inversion of Geophysical and Geological Data." Participating companies are Placer Dome, BHP, Noranda, Cominco, Falconbridge, INCO, HBE&D, Kennecott, Newmont, WMC, and CRA Exploration. We thank Cam DeLong for supplying the geologic cross-section at 9600N and thank Cliff Stanley and Cam Delong for providing information on the geochemistry of Mt. Milligan and for patiently explaining the results to us. We are grateful to Dale Sketchley and Peter Kowalczyk for providing much of the background information about Mt. Milligan and helping us piece together a consistent interpretation. We thank Placer Dome for providing the 3-D gold model and drill-hole results and both Noranda and Placer Dome for providing the geophysical data.

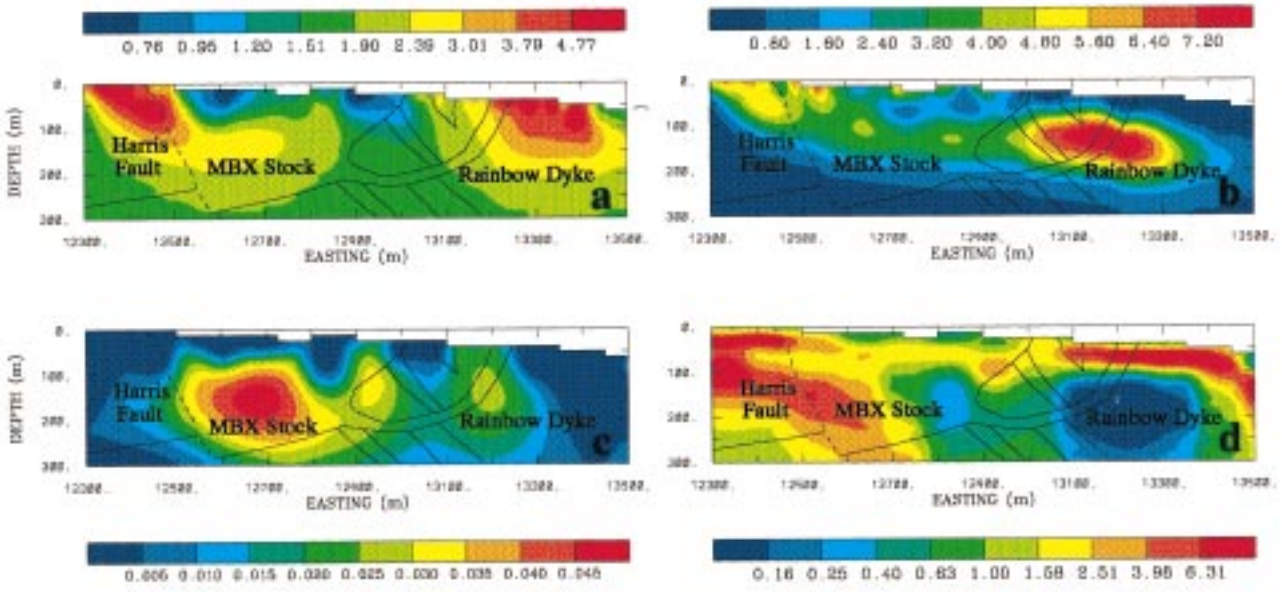

FIG. 12. Overlay of the geology onto recovered conductivity from the DC inversion (a), chargeability from IP inversion (b), susceptibility from magnetic inversion (c), and conductivity from airborne EM inversion (d). The surface topography is shown at the top of each model. The respective color scales indicate conductivity in mS/m, chargeability as percentage, and susceptibility in SI units. Notice that the low conductivity and high susceptibility correlate with the monzonite stock, while high chargeability correlates with the boundaries of the stock and dyke.

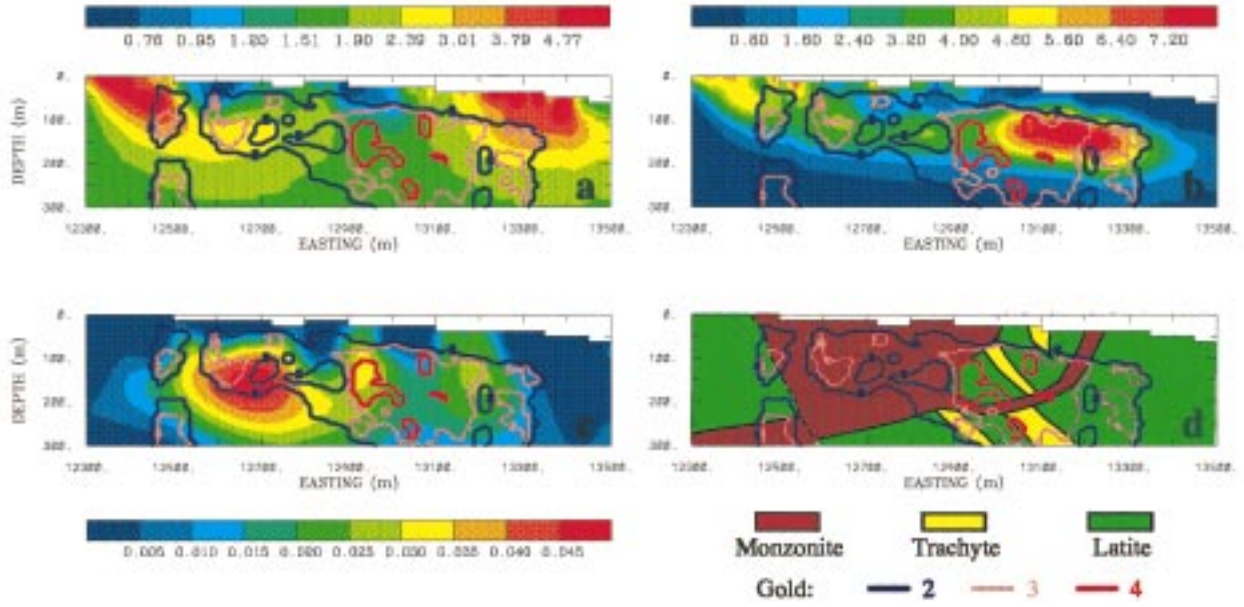

FIG. 13. Overlay of gold concentration onto recovered conductivity (a), chargeability (b), susceptibility (c), and geology (d). The gold concentration is given by categories 1 through 4, with 4 indicating the highest value. The respective color scales indicate conductivity in mS/m, chargeability as a percentage and susceptibility in SI units. Notice that the high gold concentration is associated with relatively low conductivity and susceptibility and with high chargeability.

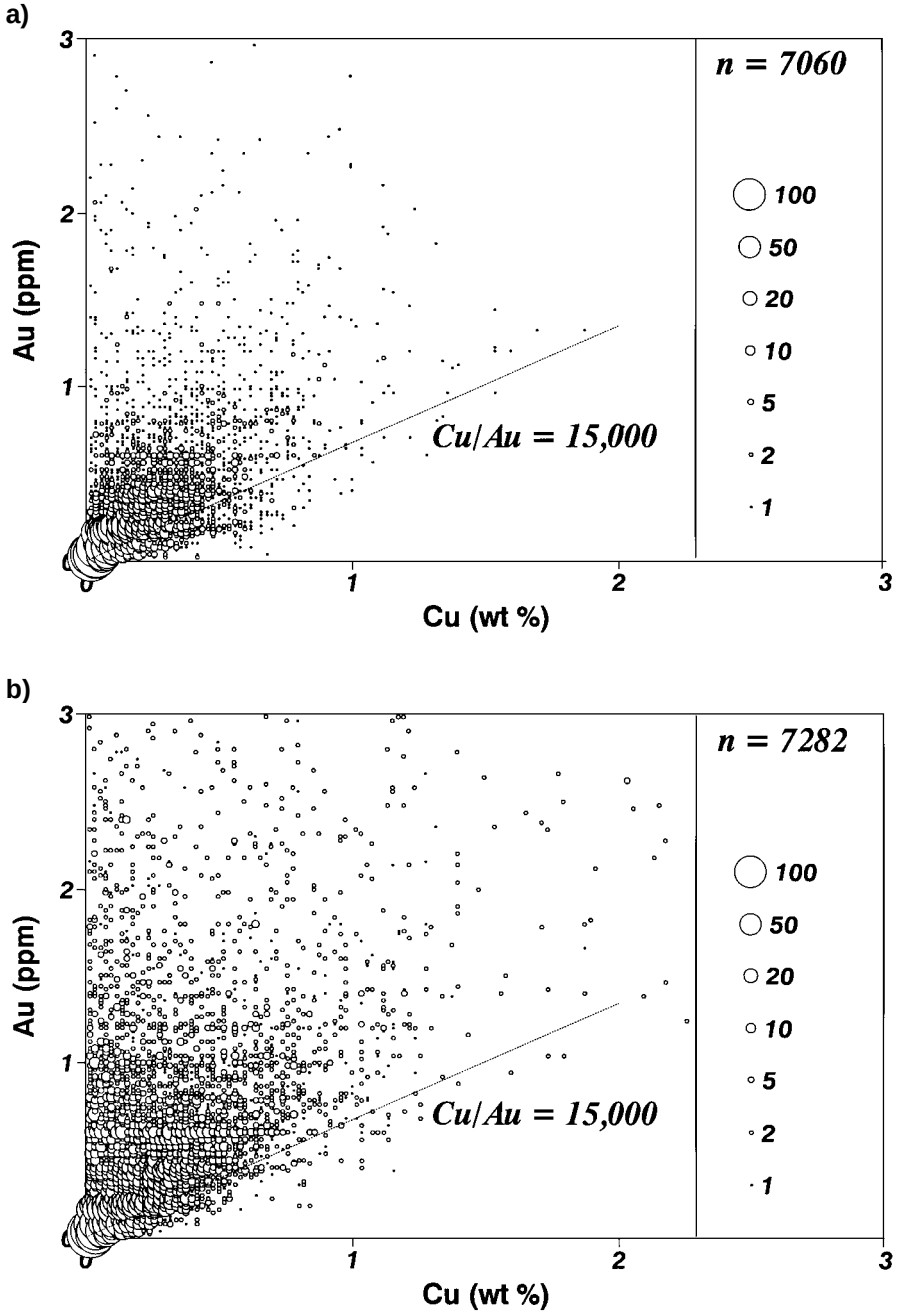

FIG. 14. Cu-Au abundances for the MBX West Zone is shown in (a). The relatively high Cu-Au correlation and magnitude of the modal Cu/Au ratio suggest that a single, high temperature potassic alteration Cu-Au mineralization event occurred in this area. In contrast, the less well-correlated concentrations for the MBX East Zone shown in (b), suggest that more than one mineralization event occurred there. An overprinting propylitic alteration Au-only mineralization event resulted in the displacement of samples upward, off the line corresponding to a Cu/Au ratio of 15 000 which probably approximates the distribution of these samples after they were affected by the earlier, high temperature Cu-Au mineralization event. Bubble sizes are proportional to sample frequency and the figures are obtained from Stanley (1993).

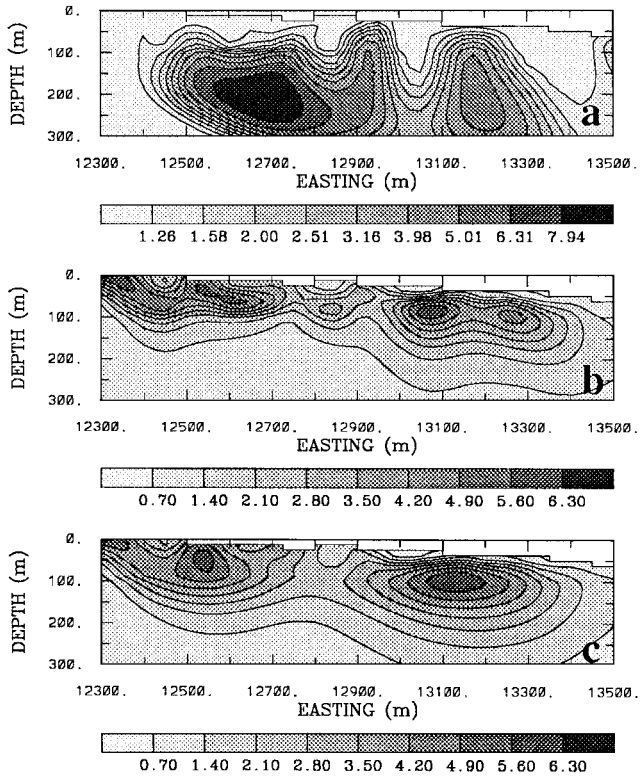

FIG. 15. Cooperative inversion of magnetic and IP data. A cross-section of a 3-D weighting function obtained from the inversion of magnetic data is shown at the top. This weighting is used in a 3-D inversion of IP data and a cross-section of the recovered chargeability at 9600N is shown in the middle panel. That model can be compared with the model at the bottom that was the original inversion of the IP data along that line.

REFERENCES

DeLong, R. C., Godwin, E. I., Harris, M. W. H., Caira, N. M., and Rebagliati, C. M., 1991, Geology and alteration at the Mt. Milligan Gold-Porphyry Deposit, Central British Columbia, *in* Geological Fieldwork 1990, British Columbia Ministry of Energy, Mines, and Petroleum Resources—Geological Survey Branch, Paper 1991-1, 199–205.

Ellis, R. G., and Shekhtman, R., 1994, ABFOR1D & ABINV1D: Programs for forward and inverse modeling of airborne EM data: JACI 1994 Ann. Rep., Dept. of Geophysics and Astronomy, Univ. of British Columbia.

Li, Y., and Oldenburg, D. W., 1996, 3-D inversion of magnetic data: Geophysics, **61**, 394–408.

McMillan, W. J., 1991, Porphyry deposits in the Canadian Cordillera, *in* Ore Deposits, Tectonics, and Metallogeny in the Canadian Cordillera, W. J. McMillan et al., Eds., Ministry of Energy, Mines and Petroleum Resources, Province of British Columbia, 253–276.

Oldenburg, D. W., and Li, Y., 1994, Inversion of induced polarization data: Geophysics, **59**, 1327–1341.

Oldenburg, D. W., McGillivray, P. R., and Ellis, R. G., 1993, Generalized subspace methods for large scale inverse problems: Geophys. J. Int., **114**, 12–20.

Stanley, C. R., 1993, A thermodynamic geochemical model for the coprecipitation of gold and chalcopyrite in alkalic copper-gold deposits: MDRU Ann. Tech. Rep., Dept. of Geological Sciences, Univ. of British Columbia.